Examples of adaptive peak tracking as found in the fossil record

Rolf Ergon

rolf.ergon@usn.no

University of South-Eastern Norway

December 7, 2025

Abstract

Species that have persisted over millions of years have done so because they have been able to track peaks in an adaptive landscape well enough to survive and reproduce. Such optima are defined by the mean phenotypic values that maximize mean fitness, and they are predominantly functions of the environment, for example the sea temperature. The mean phenotypic values over time will thus predominantly be determined by the environment over time, and the trait history may be found in the fossil record. Here I use fossil data from three cases found in the literature, and I show that adaptive peak tracking models give better results than alternative weighted least squares and directional random walk models. The model performances are compared by use of weighted mean squared errors and Akaike information criterion results.

Keywords: adaptive landscape, adaptive peak tracking, AIC, fitness landscape, fossil record, WMSE

1 Introduction

Adaptive peak tracking is known from various engineering applications, but tracking models are also relevant in evolutionary biology settings. They are then based on an adaptive landscape metaphor, which assumes that the mean population fitness in a population is a function of possibly multivariate mean phenotypic traits, with an optimum (adaptive peak) for a specific set of mean traits. See Pigliucci (2013) for historical background and clarifying discussion. Below, I also make use of an individual fitness landscape spanned by axes for individual phenotypic values, for example body size or breeding time. Here, individual fitness is a measure of reproductive success, i.e., to which degree genes are passed on to future generations. For species with sexual reproduction the phenotypic values are midparent values, i.e., the means of male and female values.

It has for a long time been known that populations and species of larger size are found in colder environments, while populations and species of smaller size are found in warmer regions. This is called Bergman's rule after the German biologist Carl Bergman, who described the pattern in 1847. Although there are exceptions from this rule, it is today referred to also in cases where a gradual change in temperature leads to gradual changes in body size, and it is then at least implicitly assumed that the body size tracks a peak in an adaptive landscape. As shown by the first real data example in Section 4, such tracking of environmental change is not restricted to body size, although it indirectly may be so.

Adaptive peak tracking in evolutionary biology can be described by the block diagram in Fig. 1. From a possibly multivariate environment $u(t)$ follows a peak $\theta_i(t)$ in the individual fitness landscape, i.e., individual phenotypic values that maximize fitness, and when $u(t)$ changes the position of this peak will change accordingly. This will again result in a moving adaptive peak $\theta_p(t)$ in the adaptive landscape, which with a non-symmetrical individual fitness function will have a different position than $\theta_i(t)$. As discussed in Ergon (2025), the two peaks may also have

different locations owing to constraints on the phenotypic values, and conceivably also for other reasons. The essential feature of the model in Fig. 1 is that the tracking process seeks to keep the mean phenotypic trait $\bar{y}(t)$ equal to the adaptive peak value $\theta_p(t)$. In the real data cases in Section 3 we will find that $\theta_p(t)$ are nearly linear functions of a dominating environmental driver, which means that also $\bar{y}(t)$ are linear functions of $u(t)$. As will be seen in real fossil data cases in Section 3, the environmental variables may be quite noisy, and I will therefore use moving average filtered signals $u_{filt}(t)$. This also a way to handle errors in the estimated age of the fossil.

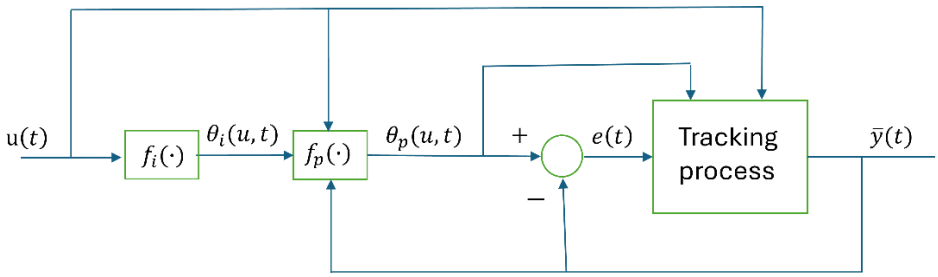

Figure 1. Block diagram for adaptive peak tracking system in evolutionary biology.

In the following I will focus on adaptive peak tracking systems involving fossil data over millions of years. An example is found in Ergon (2025), using fossil data over 2.3 million years on the relative size of feeding zooids (autozooids or AZ, see Fig. 2) in encrusting cheilostome bryozoans (Liow et al., 2024). Liow and her coworkers collected 985 fossil colonies as shown in Fig. 2, with a large total number of individual bryozoans. They summarized the results as nine *log AZ area mean* values with standard errors, see panel B in Fig. 3.

In addition to mean trait standard errors as shown by error bars in Fig. 3, there are considerable errors in the nine time points. This is because mean trait values are found as mean values of mean values for various numbers of colonies found in nine different geological formations with various time spans, and the nine time points are estimated midpoints for these formations. The dominating environmental driver is the sea temperature, with oxygen isotope $\partial^{18}O(t)$ values used as proxy (Lisiecki and Raymo, 2005). The $\partial^{18}O(t)$ values increase when the

temperature decreases, and they can be converted to temperature by linear transformations (Evans et al., 2024). Because of the potentially large time point errors in the mean phenotype data, Ergon (2025) used $u_{filt}(t)$ as a centered moving average filtered version of $\partial^{18}O(t)$. Using the moving average window size as a tuning variable, the nine mean phenotypic values fell quite nicely on a straight line (Fig. 3, panel C), and from weighted least squares (WLS) parameter estimation thus followed continuous predictions of the mean trait values (Fig. 3, panel A). Note that a high $\partial^{18}O(t)$ value means low temperature, and that the AZ area thus in accordance with Bergman's rule increases when the temperature decreases. See Section 3 for detailed results regarding the ovicell (OV) trait as shown in Fig. 2.

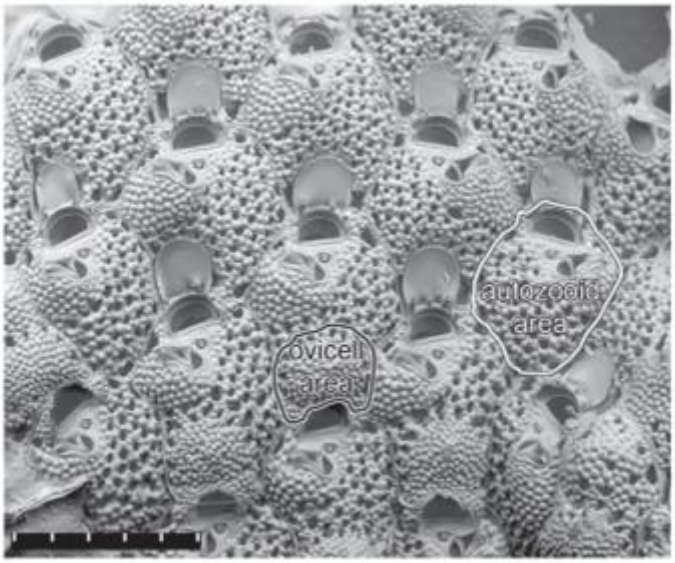

Figure 2. Scanning electron micrograph showing part of a *Microporella agonistes* colony, with perimeters of autozooid (AZ) and ovicell (OV) areas outlined. The length of the scale bar is 500 μm. From Liow et al. (2024).

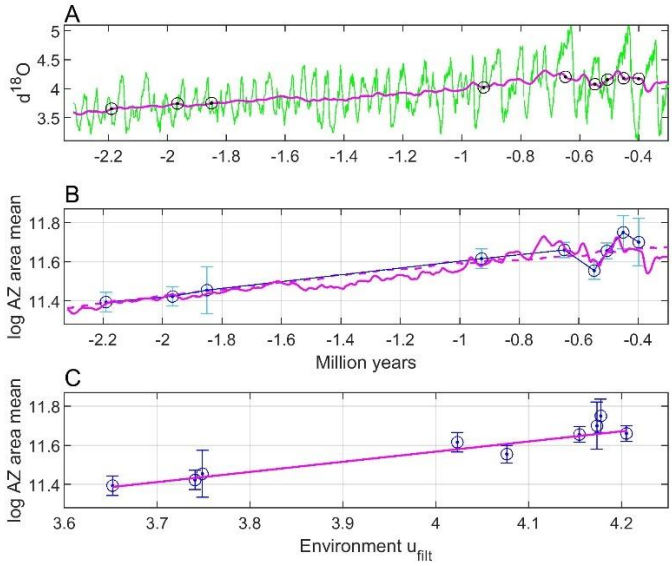

Figure 3. Results for the bryozoan species *Microporella agonistes*, as shown in Fig. 2. Panel A shows raw $\partial^{18}O(t)$ data (green line) and a centered moving average filtered version $u_{filt}(t)$ with window size 100 samples (red line). Panel B shows *log AZ area mean*, with error bars as found from Fig. S2 in Liow at al. (2024) (blue circles with dots and blue line), as well as predictions (red line). Panel C shows the estimated adaptive peak function (red) computed by the weighted least squares method. Panel B also shows predictions with window size 800 samples (dashed red line).

The adaptive peak tracking model in Fig. 1 is useful only if the following error $e(t)$ is kept sufficiently small, such that the mean phenotypic value stays in the vicinity of the adaptive peak. As discussed in Ergon (2025) this is often the case. A persistent system excitation in the form of short-term environmental fluctuations as exemplified in Fig. 3, panel A, makes it unlikely that a tracking system gets stuck in a local optimum or in a valley in the adaptive landscape. As illustrated in simulations in Ergon (2025), it is more likely that the mean phenotypic values fluctuate around global optima.

Under the assumption that the following error $e(t)$ in Fig. 1 is kept sufficiently small, such that $\bar{y}(t) \approx \theta_p(t)$, the adaptive peak function $\theta_p(t) = f\big(u(t)\big)$ can be identified from $u(t)$ and $\bar{y}(t)$

data, and that is especially simple when this function is linear. As illustrated in Fig. 3 it is then possible to find the adaptive peak function from a few and irregularly spaced data points, and thus also to predict the mean trait values $\bar{y}(t)$. Note that this can be done without detailed knowledge of the tracking process in Fig. 1.

Section 2 describes the methods used in the article. As also used in Liow et al. (2024), a well-established method for analyses of fossil time series data is to find optimal biased or unbiased random walk models (Hunt, 2006a). Biased or general random walk (GRW) models are also known as directional evolution models (Hunt, 2012). An alternative model for directional evolution is to use WLS directly on the $\bar{y}(t)$ data. In the real data cases in Section 3 I will thus compare three models, (i) tracking with use of WLS on the adaptive peak function $\bar{y}(u_{filt})$, (ii) WLS directly on $\bar{y}(t)$, and (iii) GRW. The performance of these models will be compared by use of weighted mean squared errors (WMSE). The models are also compared by use of the Akaike Information Criterion (AIC), which is often used for comparison of different random walk models of fossil data (Hunt, 2006).

In Section 3, the different methods are applied on three real case data sets in the fossil record. The first is a stickleback fish study in Bell et al. (1985), which shows that tracking of environmental change is not restricted to body size traits. The second is a study of the ostracod species *Poseidonamics major* in Hunt and Roy (2006), while the third is the already introduced field study of the bryozoan species *Microporella agonistes*, with results as in Fig. 3, but now with use of data for the ovicell (OV) area as shown in Fig. 2. Finally follows a summary and discussion in Section 4.

2 Theory and Methods

2.1 Essential elements of the tracking process

It is not necessary to know the details of the tracking process in Fig. 1, but it must have two essential elements. First, there must be a mean fitness function such that $\bar{W}(t) \rightarrow \bar{W}_{max}$ when $\bar{y}(t) \rightarrow \theta_p(u,t)$. This function defines the adaptive peak, and in the univariate case it can for example be (as in Ergon, 2025)

$$\bar{W}(t) = W_{max}\sqrt{\frac{\omega^2}{\omega^2+\sigma_y^2(t)}}\exp\left(-\frac{\left(\bar{y}(t)-\theta_p(u,t)\right)^2}{2\left(\omega^2+\sigma_y^2(t)\right)}\right), \tag{1}$$

where $\sigma_y^2(t)$ is the variance of $y(t)$, while ω^2 is the width of the underlying individual fitness function. Second, there must be a selection mechanism, such that individuals with high fitness get the best chance for reproduction (Lande, 1979). A simple example of such a set of selection equations is given in Ergon (2025). This will result in slow evolution with small changes in $\bar{y}(t)$ from generation to generation, but in addition there may be mutations that give sudden and positive jumps in the individual fitness (Ch. 7, Walsh and Lynch, 2018).

2.1 Weighted least squares estimation for tracking models

In the tracking method, least squares predictions are found as $\hat{\bar{y}}_{track}(i) = \hat{a}_{track} + \hat{b}_{track}\left(u_{filt}(i) - u_{filt}(1)\right)$, where $u_{filt}(i)$ is moving average filtered version of the $\partial^{18}O$ measure at the N sampling points. Here, the parameters are found as

$$\begin{bmatrix}\hat{a}_{track}\\ \hat{b}_{track}\end{bmatrix} = (\boldsymbol{X}^T\boldsymbol{W}\boldsymbol{X})^{-1}\boldsymbol{X}^T\boldsymbol{W}\boldsymbol{y}, \tag{2}$$

where $\boldsymbol{X} = \begin{bmatrix}1 & 1 & \cdots & 1\\ u_{filt}(1)-u_{filt}(1) & u_{filt}(2)-u_{filt}(1) & \cdots & u_{filt}(N)-u_{filt}(1)\end{bmatrix}^{\boldsymbol{T}}$ and $\boldsymbol{y} = [\bar{y}(1) \quad \bar{y}(2) \quad \cdots \quad \bar{y}(N)]^{\boldsymbol{T}}$, while $\boldsymbol{W}$ is a diagonal matrix with weights $w_i = \sigma_i^{-2}$ that are the reciprocals of the measurement variances. From this follows continuous predictions

$$\hat{\bar{y}}_{track}(t) = \hat{a}_{track} + \hat{b}_{track}\left(u_{filt}(t) - u_{filt}(1)\right), \tag{3}$$

such that $\hat{\bar{y}}_{track}(t)$ becomes a filtered and scaled version of the environmental variable.

2.2 Weighted least squares estimation for direct WLS models

In the direct WLS method, least squares predictions are found as $\hat{\bar{y}}_{track}(t) = \hat{a}_{WLS} + \hat{b}_{WLS}t$. Here, the parameters are found as in Eq. (2), except that $\boldsymbol{X} = \begin{bmatrix} 1 & 1 & \cdots & 1 \\ t_1 & t_2 & \cdots & t_N \end{bmatrix}^{\boldsymbol{T}}$, where t_i are the sample time points

2.3 Random walk models

Hunt (2006) developed what he called a general random walk (GRW) model for analyses of fossil time series, later referred to as a model for directional evolution (Hunt, 2012). This model assumes a random walk process where at each timestep an increment of evolutionary change in a mean trait value is drawn at random from a distribution of evolutionary steps, and that this incremental change is normally distributed with mean value μ_{step} and variance σ^2_{step}. For an observed evolutionary mean trait change ΔY over T time steps, the log-likelihood function for a GRW process is given by (Hunt, 2006)

$$\ell\left(\mu_{step}, \sigma^2_{step}\right) = -\frac{1}{2}\ln(2\pi) - \frac{1}{2}\ln\left(\mathrm{T}\sigma^2_{step} + \frac{V_{p_A}}{n_A} + \frac{V_{p_D}}{n_D}\right) - \frac{\left(\Delta\mathrm{Y} - \mathrm{T}\mu_{step}\right)^2}{2\left(\mathrm{T}\sigma^2_{step} + \frac{V_{p_A}}{n_A} + \frac{V_{p_D}}{n_D}\right)}, \tag{4}$$

where n_A and n_D are the numbers of observed ancestors and descendants, respectively, while V_{p_A} and V_{p_D} are the corresponding population phenotypic variances. With N irregular and sparse samples of mean trait values, multiple ancestor-descendant trait differences over $N-1$ evolutionary transitions may be used jointly to estimate μ_{step} and σ^2_{step} by summing the log-likelihoods according to Eq. (4) over the transitions, i.e., by use of $\ell_{total}\left(\mu_{step}, \sigma^2_{step}\right) = \sum_{i=1}^{N-1} \ell_i\left(\mu_{step}, \sigma^2_{step}\right)$. From this expression, step parameters can be found by means of maximum likelihood estimation, and the estimated step size $\hat{\mu}_{step}$ will then be a

measure of directional change over time. In the real data examples in Section 3, the optimal GRW parameters are found by use of the MATLAB function *fmincon*, with initial parameter values sat to zero.

The GRW model has two obvious weaknesses. One is that it is difficult to estimate σ_{step}^2 for small values of T and large values of V_{p_A}/n_A and V_{p_D}/n_D. In all of the three examples in Section 3 the result is $\hat{\sigma}_{step}^2 < 0$, such that the step variance must be set to $\hat{\sigma}_{step}^2 = 0$. The other difficulty is that for $\sigma_{step}^2 = 0$ and equal values of V_{p_A}/n_A and V_{p_D}/n_D for all transitions, the parameter estimate $\hat{\mu}_{step}$ will be determined by the first and last samples only.

Eq. (4) is not intended for predictions, but once $\hat{\mu}_{step}$ is determined with $\hat{\sigma}_{step}^2 = 0$, a prediction model

$$\hat{\bar{y}}_{GRW}(t) = \hat{a}_{GRW} + \hat{b}_{GRW} t \tag{5}$$

is found by use of $\hat{b}_{GRW} = c\hat{\mu}_{step}$, and by fitting a parameter a_{GWR} to the data by a least squares approach. Here, c is a scaling constant that I consistently will set to $c = 1$.

2.4 Weighted mean squared errors

Comparisons of responses $\hat{\bar{y}}_{track}(t)$, and $\hat{\bar{y}}_{WLS}(t)$ and $\hat{\bar{y}}_{GRW}(t)$ can be done by use of weighted mean squared errors

$$WMSE = (\bar{\boldsymbol{y}} - \hat{\bar{\boldsymbol{y}}})\boldsymbol{W}(\bar{\boldsymbol{y}} - \hat{\bar{\boldsymbol{y}}})/\sum w_i, \tag{6}$$

where $\bar{\boldsymbol{y}}$ and $\hat{\bar{\boldsymbol{y}}}$ are $N \times 1$ data vectors, and where $\boldsymbol{W}$ is a diagonal matrix with the weights w_i. Note that we in the special ordinary least squares (OLS) case have $\boldsymbol{W} = \boldsymbol{I}$ and $\sum w_i = N$. I thus assume independent and normally distributed random variables $\bar{y}(t)$. Note that when the weights are the reciprocals of the variances of the measurements, as done here, the prediction slope parameters $\hat{b}_{track}$ and $\hat{b}_{WLS}$ are the best linear unbiased estimates (BLUE).

2.4 Theory for the Akaike Information Criterion

Model performances may be compared by use of the Akaike information criterion (AIC), and the model with the lowest AIC value should then be chosen (Hunt, 2006). For GRW, the AIC value with compensation for short data is given by (Hunt, 2006),

$$AIC_{c,GRW} = 2k - 2\ell_{total}\left(\hat{\mu}_{step}, \hat{\sigma}^2_{step}\right) + 2\mathrm{k}(\mathrm{k}+1)/(\mathrm{N}-\mathrm{k}-2)\,, \tag{7}$$

where $\mathrm{k} = 2$ is the number of estimated parameters, while N is the number of samples (the number of transitions is $\mathrm{N} - 1$). Since in all the real data examples in Section 3 the estimated variance $\hat{\sigma}^2_{step}$ is negative, the realistic value of $AIC_{c,GRW}$ is found by setting $\sigma^2_{step} = 0$.

For comparisons with tracking and WLS models, Eq. (7) must be replaced by (Banks and Joyner, 2017)

$$AIC_c = 2k - 2\ln\left(\mathcal{L}\left(\widehat{\Theta}_{MLE}|\overline{\boldsymbol{y}}\right)\right) + 2\mathrm{k}(\mathrm{k}+1)/(\mathrm{N}-\mathrm{k}-1), \tag{8}$$

where $\mathcal{L}(\widehat{\Theta}_{MLE}|\overline{\boldsymbol{y}})$ is the likelihood of the estimated parameters using maximum likelihood estimation, given the vector $\overline{\boldsymbol{y}}$ of observed data. Banks and Joyner (2017) further assume a statistical model $Y_i = f(t_i, \boldsymbol{q}_0) + \omega_i \mathcal{E}_i$, where $\boldsymbol{q}_0$ is a parameter vector, while ω_i are known weights and ε_i, $i = 1, 2, \ldots, N$, are i.i.d. $\mathcal{N}(0, \sigma^2)$, such that σ^2 must be estimated together with $\boldsymbol{q}_0$. In the present setting the weights are $\omega_i = \sqrt{1/w_i}$, and the final AIC expression in Banks and Joyner (2017) thus becomes

$$AIC = 2k + Nln(2\pi) + N + 2\sum_{i=1}^{N} \ln\left(\sqrt{1/w_i}\right) + Nln\left(\frac{\sum_{i=1}^{N} w_i(\bar{y}_i - \hat{\bar{y}}_i)^2}{N}\right), \tag{9}$$

from which $AIC_{c,track}$ and $AIC_{c,WLS}$ follow by adding $2\mathrm{k}(\mathrm{k}+1)/(\mathrm{N}-\mathrm{k}-1)$. Here, $k = 3$, since also the underlying parameter σ^2 must be estimated in addition to a_{WLS} and b_{WLS}. Note that $\hat{\bar{y}}_i$ in Eq. (9) is the result of either a tracking model or WLS, and that Eq. (9) therefore is not valid with use of $\hat{\bar{y}}_{i,GRW}$ as found from Eq. (5).

3 Real data cases

3.1 Stickleback fish case

In this case I use data that show how the dorsal fin ray number evolved in the species *Gasterosteus doryssus*, an extinct species of a small freshwater stickleback fish that inhabited inland freshwater habitats of the North American Great Basin during the Miocene (Bell et al., 1985). See Table A1 in Appendix A for data. In the data analysis the mean trait values are log-transformed, with the measurement errors transformed accordingly, i.e., $e_{i,log} = e_i \cdot \frac{\bar{y}_{i,log}}{\bar{y}_i}$, where e_i is found from the given standard deviations SD as $e_i = \sqrt{SD_i^2/n_i}$. The original and log-transformed samples thus have equal coefficients of variation.

In the tracking model, the environmental driver was $\partial^{18}O(t)$ as found in Westerhold et al. (2020), Table S34, column marked ISOBENbinned_d18Ointerp. The exact sampling time points are not given in Bell et al. (1985), but since $t = 0$ in the data is approximately 10 million years ago (personal information) it was possible to align the data such that the prediction results were optimized. An optimal filter window size 96 was also found by a manual search using raw data from 9.8 to 10.3 million years ago. Since the time resolution is 0.002 million years, the moving time window size is 0.192 million years.

With σ_{step}^2 as a free variable, the term $\mathrm{T}\sigma_{step}^2 + \frac{V_{p_A}}{n_A} + \frac{V_{p_D}}{n_D}$ in Eq. (4) for one or several of the transitions becomes negative in the course of the parameter search, such that the log-likelihood becomes a complex number. The search is therefore limited to $\sigma_{step}^2 \geq 0$, resulting in $\hat{\sigma}_{step}^2 = 0$. See results in Figures 4 and 5, and in Table 1. Note that the error bars in Fig. 5 are quite equal for all samples, which as remarked in Section 2 means that $\hat{\mu}_{step}$ very much depends on the first and last samples.

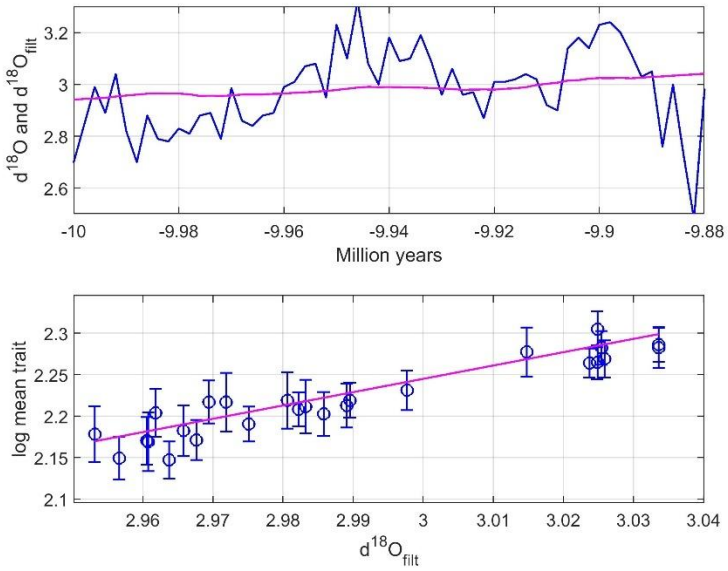

Figure 4. Plots for the Stickleback fish case. Upper panel shows $\partial^{18}O(t)$ (blue line) and $u_{filt}(t) = \partial^{18}O_{filt}(t)$ with window size 100 (red line). Lower panel shows data points $\bar{y}(i)$ and $u_{filt}(i) = \partial^{18}O_{filt}(i)$ with standard error bars, and estimated adaptive peak function line (red line).

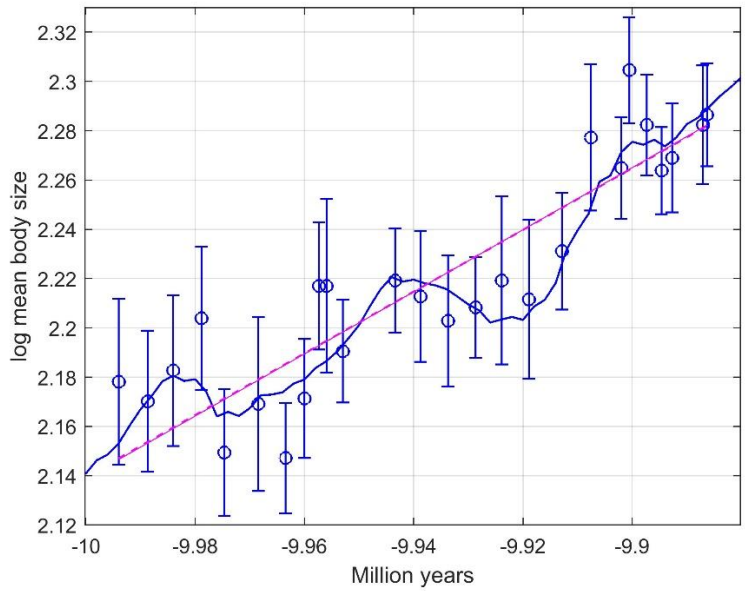

Figure 5. Tracking, WLS ,and GRW results for the Stickleback fish case, with mean trait observations (circles with standard error bars), tracking predictions (blue line), WLS

predictions (red line), and GRW predictions with $\sigma_{step}^2 \geq 0$ in the search for the optimum (dashed red line, almost identical to the solid red line).

Table 1. Prediction slope, WMSE and AIC results for predictions in Fig. 5.

	Tracking model	WLS model	GRW model
Prediction slope	–	1.2605	1.2531
WMSE	0.000216	0.000400	0.000400
AIC_c	−137	−121	−104

3.2 Ostracod case

Body size data for the deep-sea ostracod (seed shrimp) population *Poseidonamicus major* are found in Hunt and Roy (2006), Table 4, see Table A2 in Appendix A for details. The body size varies from $y = 707$ to $y = 876\ \mu m$, with the variance in the measurements estimated to be $467/n\ (\mu m)^2$, where n is the number of samples. The standard error is thus $SE = \sqrt{467/n}\ \mu m$, which on a log scale translates to $SE_{log} = \sqrt{467/n}\ \log(y)\ /y$.

The data in Hunt and Roy (2006) include Mg/Ca temperatures, but a tracking model based on this information is not any better than the WLS model. Instead, I used the environmental driver $\partial^{18}O(t)$ as found in Lisiecki and Raymo (2005), and the optimal window size was here 80. In these data the time resolution for $t > -0.6$ million years is 0.001, such that the moving time window size is 0.08 million years. For $-1.5 < t < -0.6$ the time window size is 0.16 million years, while it for $t < -1.5$ is 0.2 million years. The parameter search was also in this case limited to $\sigma_{step}^2 \geq 0$, resulting in $\hat{\sigma}_{step}^2 = 0$. See results in Fig. 6 and Table 2.

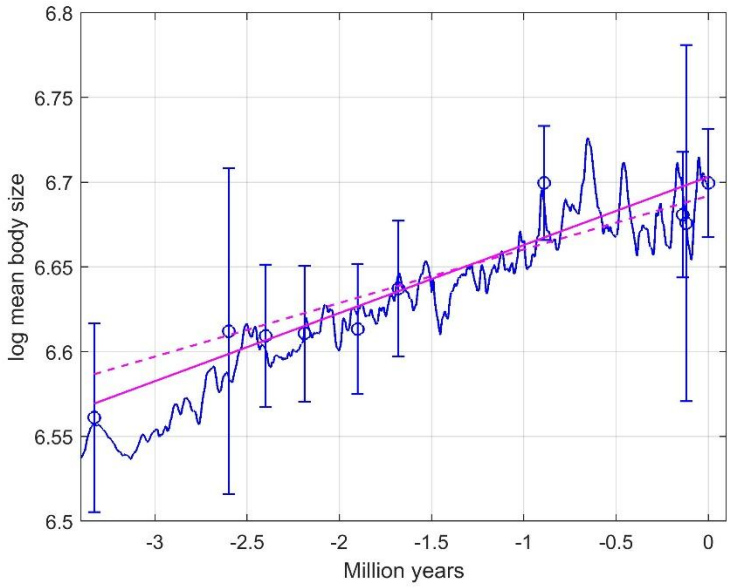

Figure 6. Tracking, WLS, and GRW results for Ostracod case, with mean trait observations (circles and error bars), tracking predictions based on $u_{filt}(t) = \partial^{18}O_{filt}(t)$ (solid blue line), WLS predictions (red line), and GRW predictions with $\sigma^2_{step} \geq 0$ in the search for the optimum (dashed red line).

Table 2. Prediction slope, WMSE and AIC results for predictions in Fig. 6.

	Tracking model	WLS model	GRW model
Prediction slope	–	0.0402	0.0316
WMSE	0.000108	0.000241	0.000319
AIC_c	−51	−43	−23

3.3 Bryozoan case 1

Liow et al. (2024) presented results from a field study of the bryozoan species *Microporella agonistes*, based on a fossil record over 2.3 million years. The scanning electron micrograph in Fig. 2 shows perimeters of autozooid (AZ) and ovicell (OV) areas, and Fig. 3 shows predictions of *log AZ area mean* as found in Ergon (2025). Fig. 7 shows the corresponding results for *log OV*

area mean. As for the results in Fig. 6, the environmental driver was $\partial^{18}O(t)$ as found in Lisiecki and Raymo (2005), and the optimal moving window size was here 700 (0.7 to 1.75 million years). The parameter search was also in this case limited to $\sigma_{step}^2 \geq 0$, resulting in $\hat{\sigma}_{step}^2 = 0$. See Table 3 for results.

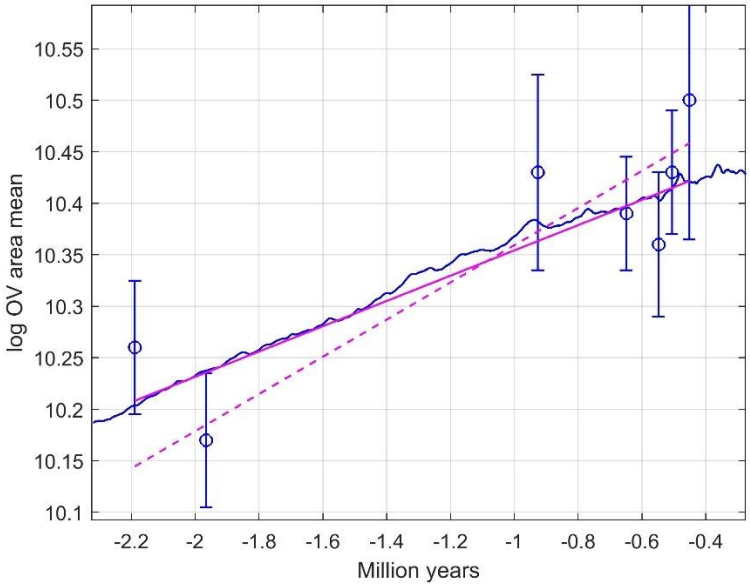

Figure 7. Tracking, WLS, and GRW results for Bryozoan case 1, with mean trait observations (circles and error bars), tracking predictions based on $u_{filt}(t) = \partial^{18}O_{filt}(t)$ (solid blue line), WLS predictions (red line), and GRW predictions with $\sigma_{step}^2 \geq 0$ in the search for the optimum (dashed red line).

Table 3. Prediction slope, WMSE and AIC results for predictions in Fig. 7.

	Tracking model	WLS model	GRW model
Prediction slope	–	0.1227	0.1805
WMSE	0.0020	0.0021	0.0038
AIC_c	−9	−8	−4

3.4 Bryozoan case 2

Finally, and for completeness, I include results from Ergon (2025), as already shown in Fig. 3, panel B. The moving window size is here 100 (0.1 to 0.25 million years). See results in Fig. 8 and Table 4. Note that there are some unfortunate errors in the AIC results given in Ergon (2025).

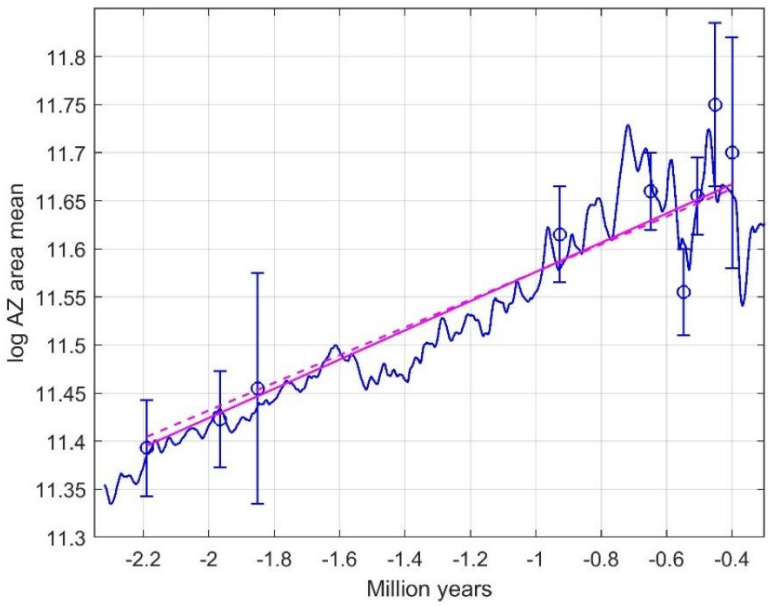

Figure 8. Tracking, WLS, and GRW results for Bryozoan case 2, with mean trait observations (circles and error bars), tracking predictions based on $u_{filt}(t) = \partial^{18}O_{filt}(t)$ (solid blue line), WLS predictions (red line), and GRW predictions with $\sigma^2_{step} \geq 0$ in the search for the optimum (dashed red line).

Table 4. Prediction slope, WMSE and AIC results for predictions in Fig. 7.

	Tracking model	WLS model	GRW model
Prediction slope	–	0.1519	0.1441
WMSE	0.0010	0.0019	0.0019
AIC_c	−23	−18	−10

4 Summary and discussion

In this article I use fossil data from three real data cases. I show that in cases with directional evolution, the adaptive peak tracking models give better results than alternative weighted least squares (WLS) and general random walk (GRW) models. The model performances are compared by use of weighted mean squared errors (WMSE) and Akaike information criterion (AIC) results.

The tracking model in Fig. 1 is in principle multivariate, although the influence from several environmental factors on the adaptive peak movements in general must be found by causal modeling that is far beyond the scope of this paper. The adaptive peak may also be influenced by non-symmetrical fitness functions and developmental constraints as discussed in Ergon (2025). In the three real data examples, positions of the adaptive peaks are approximately linear functions of temperature.

The methodological background is given in Section 2, including the theory for GRW models, and a description of how AIC values are found from WMSE results. The results for the various models are summarized in Figures 5, 6, 7 and 8, and Tables 1, 2, 3 and 4. Note that the $AIC_{c,GRW}$ values do not take the estimation of a_{GRW} in Eq. (5) into account.

In the tracking models I use oxygen isotope data for the environmental drivers. These data were found in deep sea drilling projects, and they can be converted to global ground temperatures through linear transformations (Evans et al., 2024). It is especially interesting that the first case is a study of fossils of a freshwater fish, which verifies that deep sea oxygen isotope data can be used as proxy for global temperature. This is perhaps the most convincing case when it comes to tracking model performance (Fig. 5), but it also raises questions as discussed below.

The reason for use of moving average filtering in the Bryozoan case is that the individual data are collected from geological formations with time spans from 0.019 to 0.203 million years, and

that there is a lot of variation in the raw $\partial^{18}O(t)$ data within each time window (Ergon, 2025). This is less clear in the Stickleback fish case, where possible errors in the age data are much smaller. Note, however, that the raw $\partial^{18}O(t)$ data as seen in Fig. 4, upper panel, are found from deep water drilling samples, and that the local temperature at the field site in what is now Nevada might have had rapid variations that are not captured in these data.

The stickleback fish case also illustrates an inherent difficulty with the directional evolution concept. The evolution as shown in Fig. 5 has an overall positive directional trend, but in several short time periods the evolution has a negative trend. This shows that directional evolution is not a system property, but a property of the environment. The essential system property is thus tracking, as illustrated in Fig. 1. In the linear mean trait versus environment cases studied here, the mean trait tracking predictions are simply filtered and scaled versions of the dominating environmental variable.

In the Stickleback fish case, the WLS and GRW models gave very similar results (Fig. 5 and Table 1), while the tracking model was much better. In the Ostracod case, the tracking model was clearly the best, while the GWR model gave the poorest results (Fig. 6 and Table 2). The Bryozoan case 1, with the ovicell (OV) area as shown in Fig. 2 as phenotypic trait, is special in the sense that tracking and WLS models give quite similar results (Fig. 7 and Table 3). This is not surprising since the optimal moving window is quite wide. When instead the autozooid (AZ) area was used, the tracking model was clearly best, while the WLS and GRW models gave very similar results (Fig. 8 and Table 4).

It would, finally, be interesting to find more linear cases in the literature. It would be even more interesting to find cases with non-linear mean trait versus environment functions, as discussed in Ergon (2025). The tracking methodology used here can easily be extended to handle such cases.

Acknowledgements

I thank Mike Bell for information regarding the time span of the stickleback fish data, and University of South-Eastern Norway for support and funding.

Competing interests

There are no competing interests.

Data Availability Statement

Oxygen isotope data for Figures 6, 7 and 8 are archived as *Raw data for simulations* on bioRxiv, https://doi.org/10.1101/2024.10.30.621046

References

Banks, H.T., and Joyner, M.L. (2017). AIC under the framework of least squares estimation. Applied Mathematics Letters. http://dx.doi.org/10.1016/j.aml.2017.05.005

Bell, M. A., Baumgartner, J. V., & Olson, E. C. (1985). Patterns of temporal change in single morphological characters of a Miocene stickleback fish. Paleobiology 11(3): 258-271.

Ergon, R. (2025). Adaptive Peak Tracking as Explanation of Sparse Fossil Data Across Fluctuating Ancient Environments. Ecology and Evolution. First published: 03 July 2025 https://doi.org/10.1002/ece3.71705

Evans, D., Brugger, J., Inglis, G.N., and Valdes, P. (2024). The Temperature of the Deep Ocean is a Robust Proxy for Global Mean Surface Temperature During the Cenozoic. Paleoceanography and Paleoclimatology. doi: 10.1029/2023PA004788

Hunt, G. (2006). Fitting and comparing models of phyletic evolution: random walks and beyond. Paleobiology 32: 578–601.

Hunt, G. and Roy, K. (2006). Climate change, body size evolution, and Cope's Rule in deep-sea ostracodes. PNAS, vol. 103/5: 1347–1352. www.pnas.org/cgi/doi/10.1073/pnas.0510550103

Hunt, G. (2012). Measuring rates of phenotypic evolution and the inseparability of tempo and Mode. Paleobiology, 38(3), 2012, pp. 351–373. paleo_Hunt_2012_Pb_rates.pdf

Hunt, G., Hopkins, M.J., and Lidgard, S. (2015). Simple versus complex models of trait evolution and stasis as a response to environmental change. PNAS, vol. 112 /16: 4885–4890.

Lande R (1979) Quantitative genetic analysis of multivariate evolution, applied to brain:body size allometry. Evolution 33:402-416 www.pnas.org/cgi/doi/10.1073/pnas.1403662111

Lisiecki, L. E., and Raymo, M. E. (2005). A Pliocene–Pleistocene stack of 57 globally distributed benthic δ18O records. Paleoceanography 20, A1003. doi:10.1029/ 2004PA001071

Liow, L.H., Porto, A., and Di Martino, E. (2024). Trait-Fitness Associations via Fecundity and Competition in a Two-Million-Year-Long Fossil Record. Am. Nat. 204/3. https://doi.org/10.1086/73133

Pigliucci, M. (2013). Landscapes, Surfaces, and Morphospaces: What Are They Good For? In The Adaptive Landscape in Evolutionary Biology, Eds. Svensson, E. and R. Calsbeek. Oxford University Press. https://doi.org/10.1093/acprof:oso/9780199595372.001.0001

Walsh, B., & Lynch, M. (2018). Evolution and selection of quantitative traits. Oxford University Press

Westerhold et al. (2020). An astronomically dated record of Earth's climate and its predictability over the last 66 million years. Science 369, 1383–1387. DOI: 10.1126/science.aba6853

372

Appendix A Data for real data cases

Table A1. Data for Stickleback fish case

Time	n	$\bar{y}$	SD
0	30	8.8300	0.7470
0.0053	33	8.7600	0.6630
0.0100	30	8.8700	0.6810
0.0152	36	9.0600	0.7150
0.0193	55	8.5800	0.7620
0.0256	40	8.7500	0.8990
0.0305	75	8.5600	0.7750
0.0340	52	8.7700	0.7030
0.0366	22	9.1800	0.5010
0.0381	28	9.1800	0.7720
0.0410	54	8.9400	0.6270
0.0506	45	9.2000	0.5880
0.0552	35	9.1400	0.6480
0.0603	37	9.0500	0.6640
0.0653	41	9.1000	0.5390
0.0701	25	9.2000	0.7070
0.0751	30	9.1300	0.7300
0.0811	58	9.3100	0.7540
0.0865	32	9.7500	0.7180
0.0920	84	9.6300	0.8030
0.0934	82	10.0200	0.8460
0.0967	89	9.8000	0.8280
0.0994	95	9.6200	0.7320
0.1013	57	9.6700	0.7150
0.1070	45	9.8000	0.6940
0.1077	64	9.8400	0.7180

Table A2. Data for Ostracod case

Age Ma	Mg/Ca temperature	n	Mean valve length μm
3.33	2.54	13	707
2.60	2.23	4	744
2.40	2.15	21	742
2.19	2.07	23	743
1.90	1.96	25	745
1.68	1.88	22	763
0.89	1.55	28	812
0.14	1.19	24	797
0.12	1.18	3	793
0.00	1.12	31	812

Table A3. Data for Bryozoan case 1

Age Ma	$\partial^{18}O(t)$ temperature	log AZ area mean	SE value
2.1895	3.6518	11.3930	0.0500
1.9660	3.7409	11.4230	0.0500
1.8505	3.7487	11.4550	0.1200
0.9265	4.0233	11.6150	0.0500
0.6485	4.2053	11.6600	0.0400
0.5480	4.0763	11.5550	0.0450
0.5055	4.1545	11.6550	0.0400
0.4510	4.1775	11.7500	0.0850
0.3990	4.1735	11.7000	0.1200